Journal of Power Sources 196 (2011) 9451–9458

Contents lists available at ScienceDirect

Journal of Power Sources

journal homepage: www.elsevier.com/locate/jpowsour

Experimental characterization of internal currents during the start-up of a proton exchange membrane fuel cell

A. Lamibrac, G. Maranzana*, O. Lottin, J. Dillet, J. Mainka, S. Didierjean, A. Thomas, C. Moyne

LEMTA - Nancy University - CNRS, 2 avenue de la Forêt de Haye, BP160, 54504 Vandoeuvre les Nancy Cedex, France

ARTICLE INFO

Article history:
Received 2 May 2011
Received in revised form 28 June 2011
Accepted 5 July 2011
Available online 12 July 2011

Keywords:
PEM fuel cells start-up
Modelling
Internal currents
Segmented cell
Hydrogen flow rate
Carbon corrosion

ABSTRACT

Start-up/shutdown under inappropriate conditions are known to damage proton exchange membrane fuel cells. Several measurement techniques were already used to characterize their effects and the degradations are mainly attributed to carbon oxidation: a decrease of the cathode active area is commonly observed after start-up/shut-down cycles.

In order to achieve a better understanding of the conditions in which this phenomenon appears, a segmented cell was designed and internal currents were recorded during start-up under open circuit conditions. The results of this work allow estimating the carbon losses at a global, as well as at a local scale, as a function of the hydrogen flow rate. Local electrochemical impedance spectroscopy measurements carried out on damaged MEA show clearly that the segments that remain for the longest time in the presence of air (while the others are fed by hydrogen) are the most affected by carbon oxidation.

© 2011 Elsevier B.V. All rights reserved.

1. Introduction

During the start-up of a PEMFC, the anode compartment is divided momentarily into an upstream part occupied by fresh hydrogen and a downstream part filled with the gas which was used to flush the anode: air or nitrogen. The boundary between the downstream and the upstream parts moves from the inlet to the outlet of the anode compartment with a velocity that is governed by the hydrogen flow rate. Start-ups occur generally under open circuit conditions so that positive and negative internal currents appear between the anode and the cathode. These internal currents can be observed thanks to dual cell configuration [1–3] but also with instrumented cells [4]. Their origin is attributed to faradic reactions [1,5], as depicted in Fig. 1: hydrogen is oxidized in the inlet part of the anode compartment while in the presence of oxygen, water and carbon oxidation can take place at the cathode.

Evidence of carbon oxidation was brought by measuring in real time the emissions of CO_2 in the air exiting the cathode during start/stop cycles [6–9]. Gu et al. [7] measured between 60 and 100 ppm (parts per million) for stop and start-up sequences, respectively, with hydrogen and air flow rates set to 140 sccm (standard cubic centimeters per minute) at the anode (1000 sccm for air at the cathode).

The aims of the work presented in this paper are to measure and analyze the internal currents occurring during PEMFC start-up sequences, in order to better understand their origin, their nature, and their consequences in term of cathode oxidation. These investigations are carried out by means of a segmented cell. Segmented cells are increasingly used for in situ investigation of PEM fuel cell operation [10,11], for instance to design channels [12] or to optimize their performances [13]. Although suitable for the study of degradations [14,15], they were rarely employed for characterizing start-up and shut down sequences [16]. The experimental results are interpreted by reference to an electrical equivalent circuit proposed by Maranzana et al. [17], who showed numerically that the capacitive contribution to negative currents could be significant, depending on the operating conditions. As a consequence, it appears that carbon oxidation, and thus the resulting fuel cell degradation and performance losses, depend highly on the start-up/shut-down protocol.

2. Segmented cell prototype

The experimental results presented in the following were obtained with the test bench depicted in Fig. 2. This bench was developed in order to monitor a unique cell with 20 segments. Gases are supplied through 6 mass flow controllers, which allow selecting a broad range of flow rates. All of them except nitrogen are humidified. Hydrogen and air are introduced in the cathode and anode compartment in counter-flow. The gas lines also allow

* Corresponding author. Tel.: +33 3 83 59 55 48; fax: +33 3 83 59 55 51.
E-mail address: gael.maranzana@ensem.inpl-nancy.fr (G. Maranzana).

0378-7753/$ – see front matter © 2011 Elsevier B.V. All rights reserved.
doi:10.1016/j.jpowsour.2011.07.013

Nomenclature

S	fuel cell area (cm^2)
j_{seg}	local current density ($A\,cm^{-2}$)
t	time (s)
R_∞	infinite resistance or discharge resistance (Ω)
$Q_{P\_N_2}$	passive charge for a start-up by injection of hydrogen in nitrogen (C)
Q_{P_Air}	passive charge for a start-up by injection of hydrogen in air (C)
$Q_{B\_N_2}$	balancing charge for a start-up by injection of hydrogen in nitrogen (C)
Q_{B_Air}	balancing charge for a start-up by injection of hydrogen in air (C)
$Q_{green\_area\_N_2}$	active charge + positive balancing for a start-up by injection of hydrogen in nitrogen (C)
$Q_{green\_area\_Air}$	active charge + positive balancing for a start-up by injection of hydrogen in air (C)
$Q_{A\_N_2}$	active charge for a start-up by injection of hydrogen in nitrogen (C)
Q_{A_Air}	active charge for a start-up by injection of hydrogen in air (C)
U	fuel cell voltage (V)
RH	relative humidity
HFR	high frequency resistance ($\Omega\,cm^2$)
C	capacity ($F\,cm^{-2}$)

flushing the anode with nitrogen or air, and the cathode with nitrogen.

Fig. 3 shows pictures of the instrumented cell. The anode flow field plate is in gold plated alumina. Except for the results presented in Section 3.1, the anode plate is not segmented and it is also used to control the temperature in the cell thanks to a cooling circuit and a thermostated bath (Lauda RE104-E100). The cathode compartment is machined in a polycarbonate plate (transparent but non-conductive) and the current collection is made by 20 electrically insulated segments (Fig. 3). The four 15 mm, 1 mm thick gold plated brass strips used for each segment delimit five parallel air channels (the depth and width of the 5 straight parallel channels are 0.7 mm × 1 mm, at the cathode and at the anode). Kapton sheets (2.3 mm × 1 mm × 80 μm) are used to isolate each strip from the adjacent ones. The four strips of each segment are electrically connected outside the cell, which amounts to averaging the current over the membrane's width. The local currents are measured thanks to 20 shunt resistors of 5 mΩ and recorded by a data processing and acquisition system (National Instrument SCXI multiplexer) at a frequency of 200 Hz (Fig. 4).

The 1 cm × 30 cm, not segmented, Johnson Matthey MEA consists of a Nafion 212 membrane, 0.4 $mg_{Pt}\,cm^{-2}$ electrodes and 190 μm thick gas diffusion layers (Toray paper). 150 μm Teflon gaskets are inserted between the MEA and the flow field plates. The plates are held together thanks to a set of 40 bolts tightened to a torque of about 2.5 N m.

A Labview program makes it possible to control the mass flow and the operation of the valves as functions of the experimental data: temperature, voltage and local currents. Local impedance spectroscopy was performed in galvanostatic mode with a frequency range of 0.25–800 Hz and with an amplitude of the (total) current oscillation equal to 5% of the steady state value (with a National Instrument USB 6221 load controller).

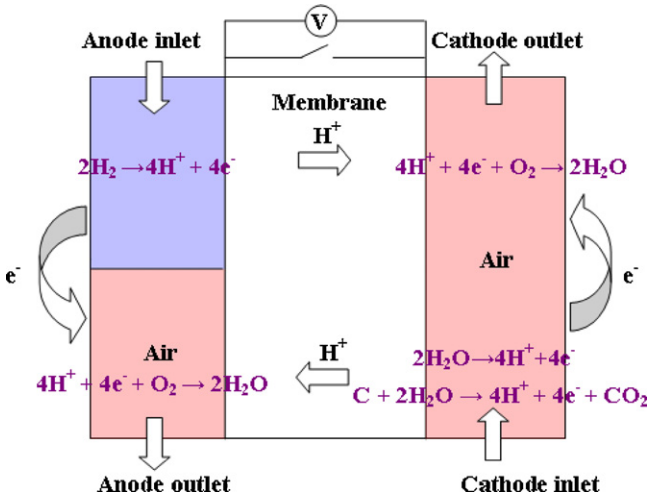

Fig. 1. Reactions occurring during start-up, the anode compartment being initially filled with air.

3. Results and discussion

3.1. Comparison of internal currents between anode and cathode during start-up

Internal currents measured at one electrode provide only partial information about the direction of the flow of the protons. Those produced in the active part of the anode should logically flow through the membrane toward the cathode. However, one cannot exclude a priori the possibility that some protons flow along the membrane to react with oxygen present in the passive part of the fuel cell (Fig. 5).

This information can be obtained by using a cell segmented on both electrodes and by comparing the internal currents measured on both sides. The results are presented in Fig. 6.

The curves in Fig. 6 show only a small discrepancy between the internal currents measured at the anode and at the cathode. This is probably due to the non-uniformity of the contact resistances between the collecting strips and the gas diffusion layers, which leads to a redistribution of the electrons between successive segments: one can check that the difference between the anode and cathode currents is exactly compensated from one segment to another. Moreover the total amount of charge produced at the anode is the same as the one consumed at the cathode (the difference is less than 3%). Consequently, the flow of protons along the membrane can be considered as negligible: using a fuel cell segmented at the cathode only makes it possible to measure accurately the internal currents.

3.2. Equivalent electrical circuit

3.2.1. Start-up with the anode compartment previously filled with nitrogen

The equivalent electrical circuit that can be used to understand and to model the occurrence of internal currents was proposed by Maranzana et al. [17] (Fig. 7). The purpose of this model is to contribute to the understanding of the phenomena governing the internal currents. Mass transport is not accounted for. For the sake of simplicity, the fuel cell is segmented into only two segments in the example described below.

Two stages can be highlighted. The *first stage* corresponds to an anode partially filled with hydrogen (Fig. 7a); the regular oxido-reduction reactions occur in the active part and in parallel, the

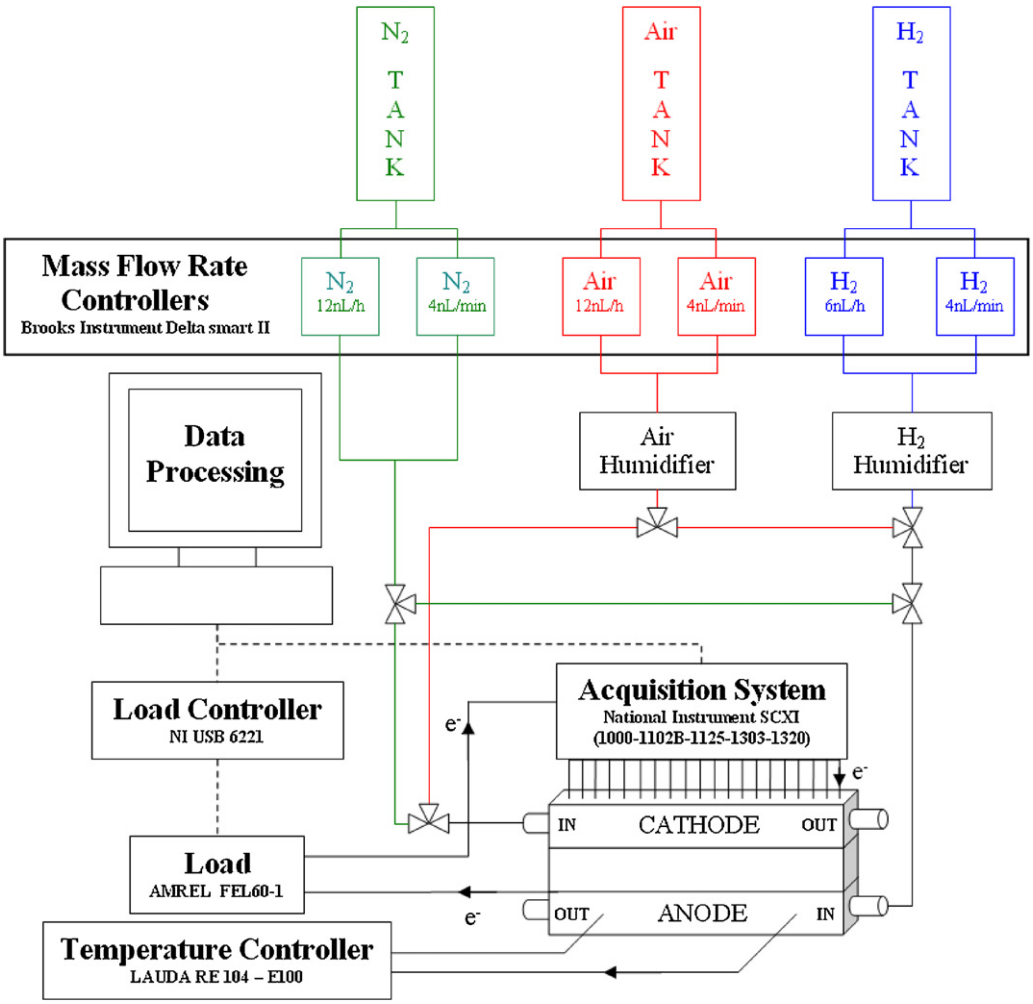

Fig. 2. Gas lines and data acquisition and processing system.

increase of the electrochemical potential leads to the charge of the double layer capacity at both electrodes.

The fuel cell being in open circuit, the electrons produced in the active part (at the anode) flow toward the passive part where negative currents (by reference to the normal fuel cell operation) are measured. In the absence of oxygen, no electrochemical reaction can occur in the passive part: these negative currents are capacitive currents. The corresponding charge of the double layer capacities is of sign opposite to that occurring in the active part.

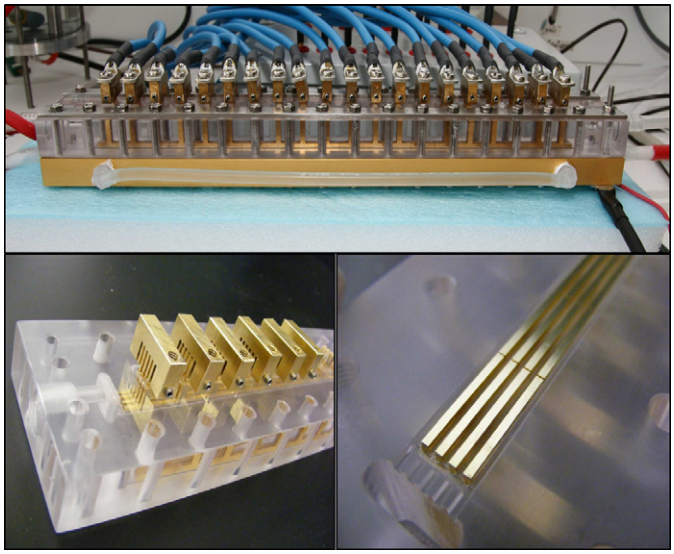

Fig. 3. Segmented cell and close-up on the current collection strips.

The *second stage* corresponds to an anode completely filled with hydrogen (Fig. 7b), that is to say to the instant the second segment becomes active when reached by hydrogen. At this time, the potential of the electrodes (of the cathode) increases up to its steady state value whereas the double layer capacities remain charged negatively (by reference to the regular operation).

As a consequence, the fuel cell voltage exceeds the open circuit value for a short time (Fig. 8); simultaneously the non-uniformity of the charge of the capacities over the whole membrane electrode assembly (MEA) gives rise to capacitive internal currents, until the complete redistribution of charges. Then, the fuel cell voltage decreases slowly down to its steady state open circuit value; this process is not yet well understood but it can be assumed that there is a small leakage current between anode and cathode, which corresponds to the resistance R_∞ (actually not infinite, but high) in parallel with the double layer capacity in the equivalent circuit.

Except for the first points, the voltage maximum value diminishes with the hydrogen flow rate, which can be explained by some variations in the charge of the double layer capacities. As far as the first points are concerned, it should be mentioned that the experiments were done from the high to the low hydrogen flow rates and by alternating air and nitrogen flushes: consequently, the results of

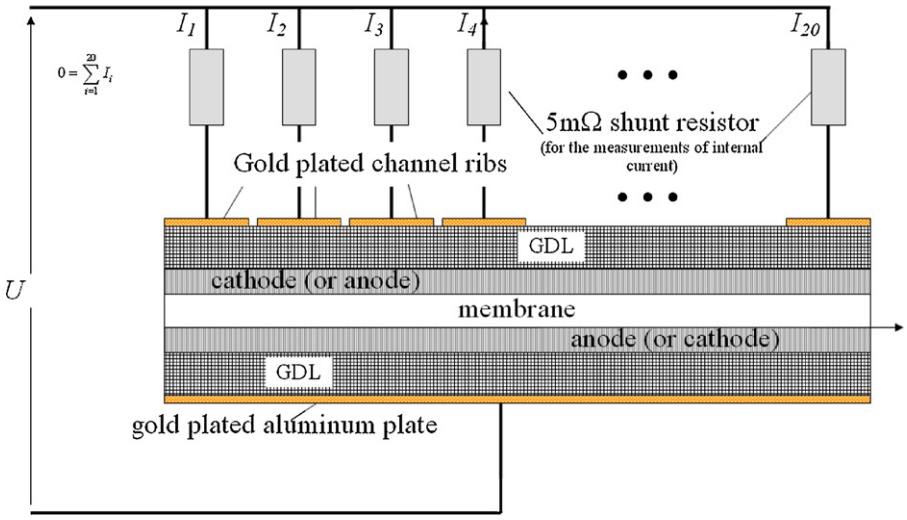

Fig. 4. Segmented cell electrical connections.

Table 1
Fuel cell voltage overshoot in the presence of nitrogen vs. hydrogen flow rate. Air and hydrogen humidified to 100% RH, fuel cell temperature set to 50 °C.

H_2 flow rate (slph)	0.1	0.2	0.5	1	2	5	10	20	30
Fuel cell overshoot (V)	1.06	1.09	1.10	1.09	1.08	1.06	1.03	1.01	1.00

the last measurements (the first points in Table 1) are affected by carbon oxidation.

Note that a voltage overshoot of 0.1 V represents 10% of the steady state OCV, and 15–20% of the fuel cell voltage in operation. A 100 cells stack designed for working at 0.6 V/cell (60 V/stack) could reach an OCV of 110 V at start-up, a value 80% higher than in regular operation: one simple way to reduce the fuel cell voltage overshoot during start-up consists in increasing monetarily the hydrogen flow rate.

3.2.2. Start-up with the anode compartment previously filled with air

The presence of oxygen in the anode compartment entails oxidation reactions at the cathode in the presence of negative currents (the cathode becoming transiently an anode during the first stage of the start-up sequence). These oxidation reactions (either oxygen evolution or carbon corrosion) correspond to a faradic contribution to the negative current density measured in the passive part; they are accounted for in the equivalent circuit with a charge transfer resistance – set in parallel to the double layer capacity – as well as with an electrode potential (Fig. 9).

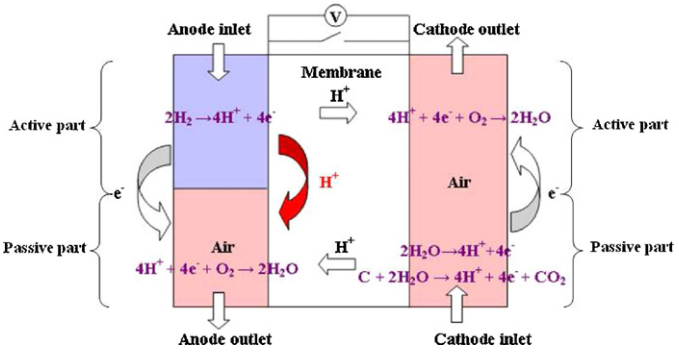

Fig. 5. Reactions occurring during start-up assuming possible flow of protons along the membrane from the active part to the passive part of the anode compartment (initially filled with air).

Note that because of the presence of air at the anode, the potential difference between the cathode and the electrolyte can reach up to 1.6 V, corresponding to very oxidizing conditions [1,5–7,18].

3.3. Experimental results: local current densities

Fig. 10a shows the evolution of the local current densities measured in all the segments during a start-up with the anode initially filled with nitrogen. We focus in the following on current density profiles measured on the first segment supplied with hydrogen (Fig. 10b), on a segment located at an equal distance from the anode inlet and outlet (Fig. 10c) and on the last segment (Fig. 10d).

The first segment supplied with hydrogen is always active while all the others become successively active once in the presence of hydrogen. The redistribution of charges begins when the faradic reactions stop. At this time, the first segment releases some of the electrons it has accumulated at the cathode—which corresponds to a negative current in Fig. 10b and c whereas the inverse phe-

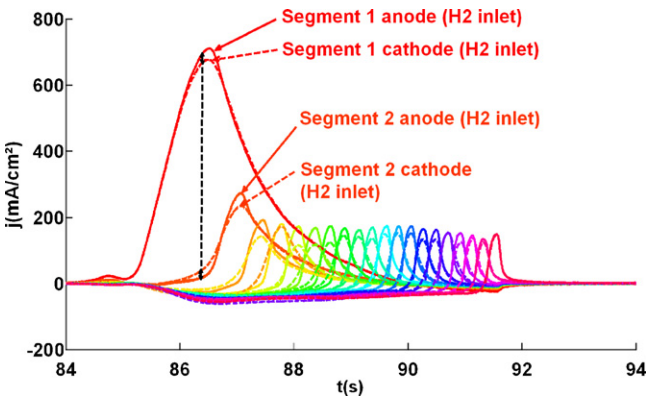

Fig. 6. Local current densities measured at the anode and at the cathode segments during a start-up with the anode compartment initially filled with air (H_2 flow rate = 2 slph, air flow rate = 20 slph). Air and hydrogen humidified to 100% RH, fuel cell temperature fixed to 50 °C.

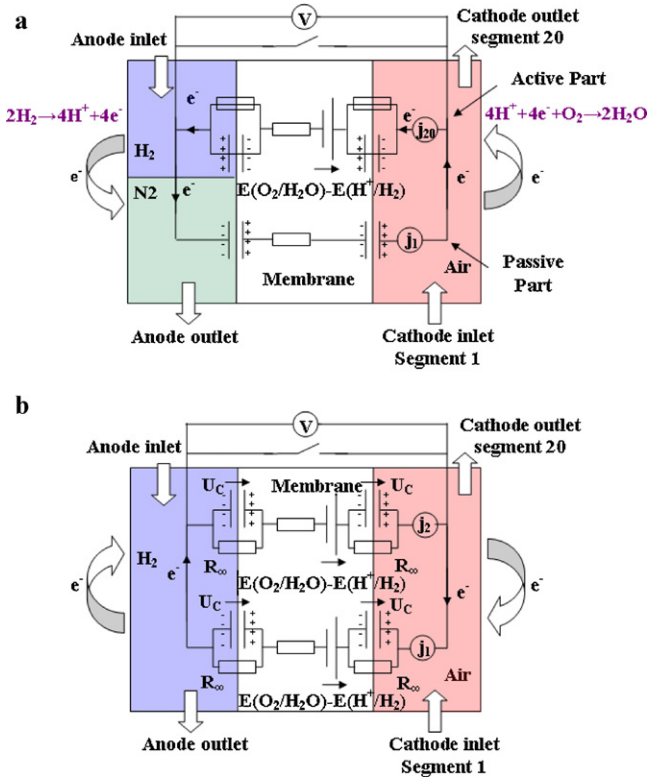

Fig. 7. (a) Equivalent electrical circuit corresponding to a start-up with the anode initially filled with nitrogen—first stage, anode partially filled with hydrogen. (b) Equivalent electrical circuit corresponding to a start-up with anode initially filled with nitrogen—second stage, anode completely filled with hydrogen.

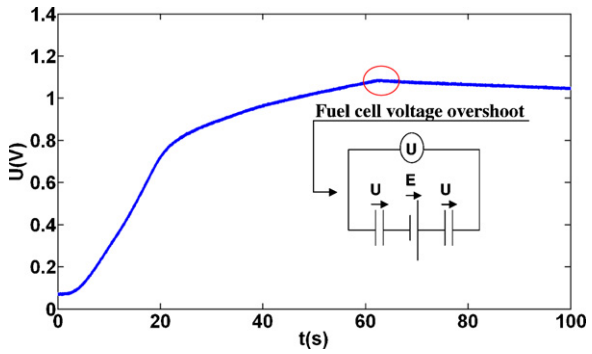

Fig. 8. Fuel cell voltage during a start-up with the anode initially filled with nitrogen—experimental results measured with a hydrogen flow rate set to 0.2 slph. Air and hydrogen humidified to 100% RH, fuel cell temperature fixed to 50 °C.

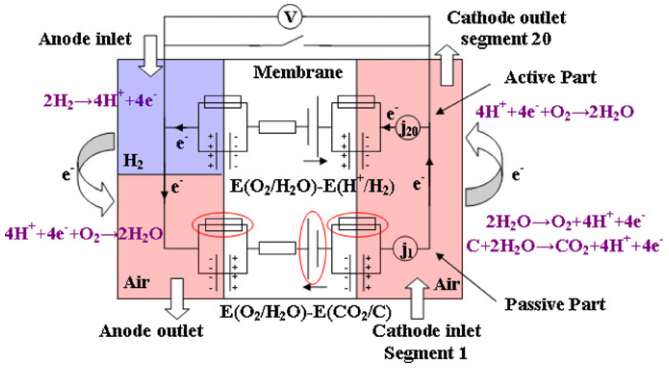

Fig. 9. Equivalent electrical circuit corresponding to a start-up with the anode initially filled with air–First stage, anode partially filled with hydrogen.

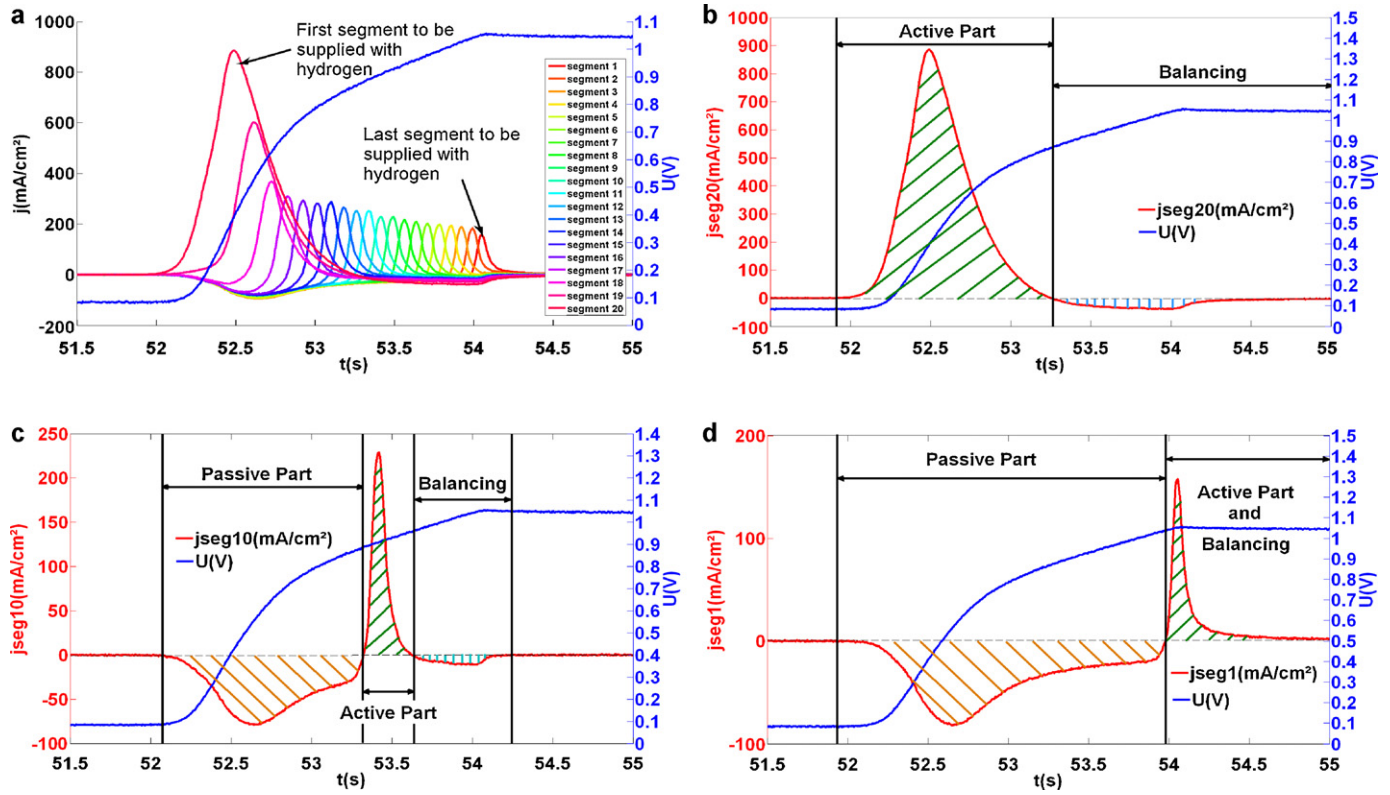

Fig. 10. (a) Current density measured in each of the 20 cathode segments and fuel cell voltage increase (vs. time) during start-up. Anode initially filled with nitrogen; hydrogen flow rate set to 5 slph. Air and hydrogen humidified to 100% RH, fuel cell temperature fixed to 50 °C. (b) Current density in the anode first segment and fuel cell voltage vs. time during start-up. (c) Current density in the anode 10th segment (of 20) and fuel cell voltage vs. time during start-up. (d) Current density in the anode last segment and fuel cell voltage vs. time during start-up.

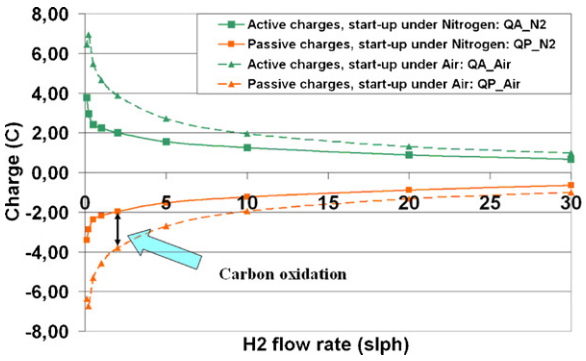

Fig. 11. Total amount of passive and active charges exchanged during a start-up sequence vs. the hydrogen flow rate. Anode initially filled with nitrogen. Air and hydrogen humidified to 100% RH, fuel cell temperature fixed to 50 °C.

nomenon occurs in the last segment. The balance of charge shows that the time and space integral of the negative currents is strictly equal to that of the positive currents. Starting from these considerations, it is possible to define three types of charge exchange during the start-up sequence:

(i) The passive charges correspond to the negative currents measured in the passive part of the fuel cell (orange hatched area in Fig. 10c and d),

$$Q_{P\_N_2} = S\sum_{i=1}^{20}\int_{\text{Passive\_part}} j_{\text{seg}(i)}\,dt < 0$$

(ii) Balancing charges are exchanged during the redistribution stage once all segments became active; the negative balancing charges correspond to the blue hatched area in Fig. 10b and c,

$$Q_{B\_N_2} = S\sum_{i=1}^{k}\int_{\text{Balancing}} j_{\text{seg}(i)}\,dt < 0$$

(iii) Active charges correspond to the positive current measured in the active part minus the positive balancing charges (equal in absolute value to the negative balancing charges),

$$Q_{\text{green\_area\_N}_2} = S\sum_{i=1}^{20}\int_{\text{Green\_area}} j_{\text{seg}(i)}\,dt$$

$$Q_{A\_N_2} = Q_{\text{green\_area\_N}_2} + Q_{B\_N_2} > 0$$

In term of MEA degradation, carbon oxidation occurs in the presence of negative currents in the passive part, i.e., it is linked to the amount of charges flowing through the passive segments (as long as they remain passive), which depends on the hydrogen flow rate and on the gas filling initially the anode compartment, as shown in Fig. 11.

The most important result in Fig. 11 concerns the significant impact of the gas filling initially the anode compartment on the amount of charge produced during the start-up sequence: it is much lower in the presence of nitrogen, this difference being attributed to the absence of a faradic contribution to the negative currents flowing through the passive segments, i.e., to the absence of carbon corrosion at the cathode when there is no oxygen at the anode.

One can also notice that the impact of air on the faradic contribution to the passive charges decreases with the hydrogen flow rates: this is probably due to the low kinetic of carbon oxidation (and possibly of oxygen evolution) compared to the capacitive current densities in the passive part.

3.4. Experimental results: carbon oxidation and performance losses

Assuming that the double layer capacities are independent of the gas in the anode compartment, and that oxygen evolution is negligible compared to carbon corrosion (which seems reasonable but has to be checked), one can estimate the mass of carbon oxidized during a start-up sequence starting from the difference between the amount of passive charges measured when the anode compartment is initially filed with air and with nitrogen.

This last result is illustrated in Fig. 12a, where one can clearly see the decrease of carbon corrosion at high hydrogen flow rate. The estimated weight of oxidized carbon per start-up is consistent with the initial amount used as catalyst support at the cathode (about 50 mg) and with the amount of carbon dioxide measured at the cathode outlet by Ofstad et al. [9].

Fig. 12b shows that the carbon loss is more important for the segments located near the hydrogen outlet, because they are submitted for a longer time to higher oxidizing conditions. As in Fig. 12a, the lower the hydrogen flow rate, the higher the amount of carbon oxidized.

The performance losses resulting from carbon oxidation can be characterized by the evolution of the fuel cell performance and of the local impedance spectra (EIS) measured along the gas channels. This was done for a succession of start/stop sequences according to three different protocols:

1. anode flushed with nitrogen, nitrogen flow rate at shut down and hydrogen flow rate at start-up set to 12 slph;
2. anode flushed with air, air flow rate at shut down and hydrogen flow rate at start-up set to 12 slph;
3. anode flushed with air, air flow rate at shut down and hydrogen flow rate at start-up set to 2 slph.

Between two successive sequences, the fuel cell current density was set to 0.5 A cm^{-2} during 1 h, with air and hydrogen humidified to 60% RH, stoichiometric ratios equal to 3 and 1.2, and a temperature fixed to 50 °C. The local impedance spectra were measured during this steady state operation.

The evolution of the fuel cell voltage as a function of the number of start-up/shut-down is depicted by the curves of Fig. 13. They show a dramatic voltage drop when the anode is flushed with air, all the more so when the hydrogen flow rate is low. Note that these experiments have been carried out with new MEA, which explains the sharp increase in performance observed during the first sequences in the three cases. When the anode is flushed with nitrogen, the improvement of the performance can be observed approximately until the 150th sequence; beyond, the fuel cell voltage at 0.5 A cm^{-2} starts to decrease slowly, probably under the effect of potential cycling associated with the various stages of the start/stop protocol.

The aging tests were stopped when the fuel cell voltage fell under 0.63 V at 0.5 A cm^{-2}. This value was reached after about 60 cycles with the third protocol (air flush at 2 slph) and 180 cycles with the second protocol (air flush at 12 slph). Starting from the results depicted in Fig. 12a, one can estimate that the corresponding carbon losses were equal to about 0.1 and 0.02 mg/start-up, respectively.

According to Gu et al. [7], the carbon loss during shut-down is approximately equal to 50% of its value during start-up, which gives

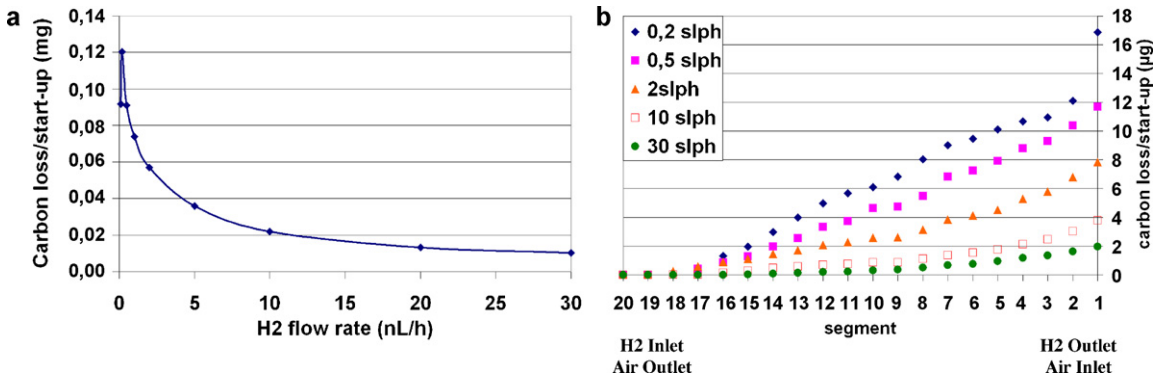

Fig. 12. (a) Estimation of the carbon loss/start-up as a function of the hydrogen flow rate. Air and hydrogen humidified to 100% RH, fuel cell temperature fixed to 50 °C. (b) Estimation of the carbon loss/start-up for each segment as a function of the hydrogen flow rate. Air and hydrogen humidified to 100% RH, fuel cell temperature fixed to 50 °C.

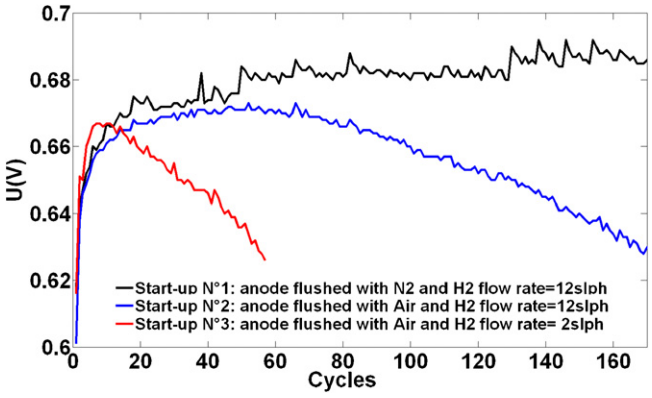

Fig. 13. Fuel cell voltage @ 0.5 A cm^{-2} vs. number of start/stop sequences following three different start/stop procedures.

us (rough) estimates of the carbon losses per start/stop sequence (0.15 and 0.03 mg, respectively) and thus over the whole aging tests: about 10 mg with the third protocol (air flush at 2 slph) and 6 mg with the second protocol (air flush at 12 slph). These values represent 10–20% of the total mass of carbon used to make the electrodes, which is in the order of magnitude of the voltage drop (about 10%, by reference to the maximum value – 0.69 V – reached with nitrogen).

Note that these estimations only tend to confirm our interpretations of the faradic and capacitive origins of negative currents. Accurate measurement of carbon oxidation and of its consequences starting from the analysis of internal currents is an objective difficult to achieve because of the complexity of this phenomenon: for instance, the production of carbon monoxide poisoning the active sites [19–22] should be taken into account, as well as the Pt coarsening resulting from carbon loss [23,24].

Finally, the evolution of the impedance spectra provides complementary information about the local effects of carbon corrosion. The results depicted in Fig. 14 correspond to the second aging protocol (air flush at 12 slph): a comparison is made between local

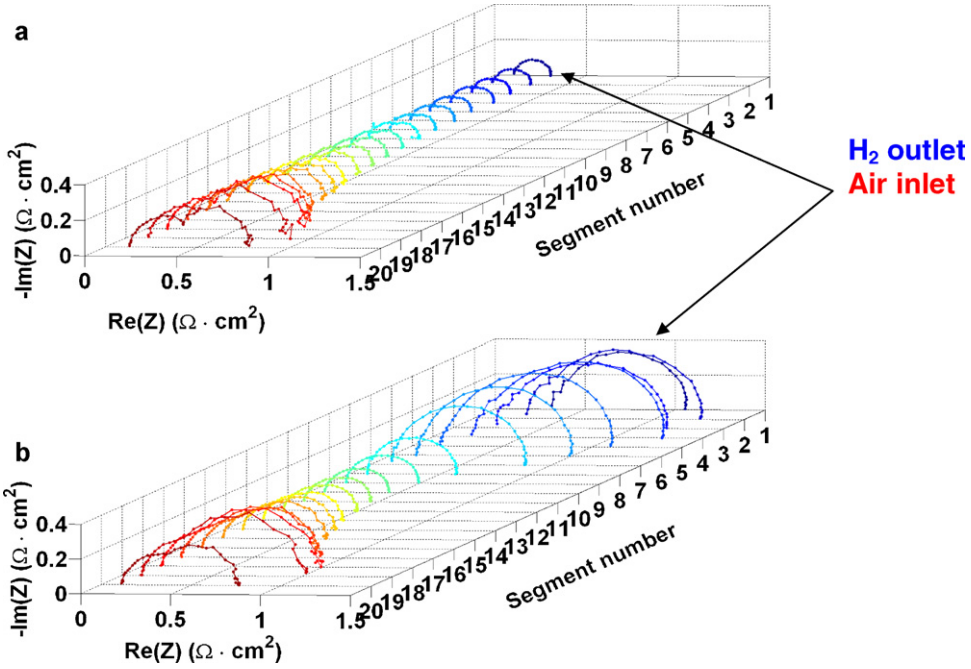

Fig. 14. (a) Local impedance spectra after 49 start/stop sequences following protocol No. 2. The cell voltage is the highest in Fig. 13. There is no visible effect of carbon corrosion. (b) Local impedance spectra after 173 start/stop sequences following protocol No. 2. The cell voltage has dropped to 0.63 V in Fig. 13 and one can observe a significant increase in the impedance of the segments located near the hydrogen outlet (the end of the anode compartment where air is introduced).

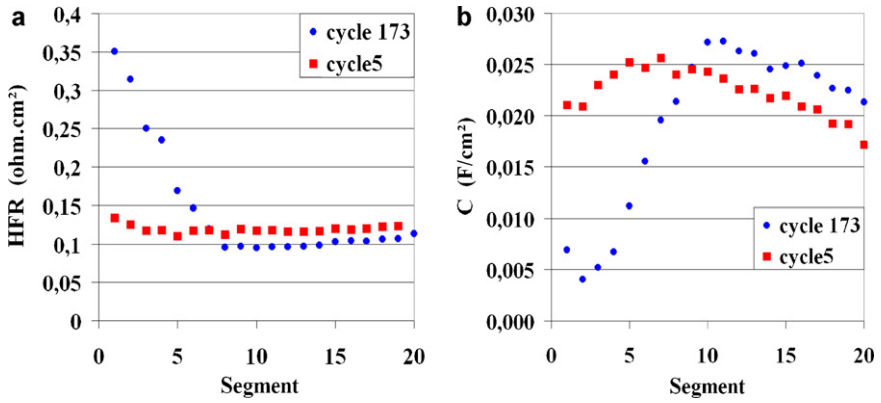

Fig. 15. (a) High frequency resistance profiles after 49 and 173 start/stop sequences following protocol No. 2. (b) Double layer capacity profiles after 49 and 173 start/stop sequences following protocol No. 2.

impedance spectra measured after 49 and 173 start/stop sequences, which confirms that the segment located near the hydrogen outlet (i.e., near the end of the anode compartment, where air is introduced) are more affected, as shown by the increase of their impedance. Nevertheless, it remains possible to fit these experimental spectra using the usual Randle's equivalent circuit and to identify the main impedance parameters [25].

A detailed analysis of their profile would be out of the scope of this paper, all the more so since the usual hypotheses and simplifications leading to the expression of the Warburg impedance are probably not adapted to model mass transport. However, it appears clearly that the high frequency resistance increases dramatically near the hydrogen outlet (Fig. 15a). This high frequency resistance is the sum of the contact resistances between the MEA components, of the protonic resistance of the electrolyte, and of the electronic resistances of the electrodes, gas diffusion layers and bipolar plates: in our case, its increase is most probably due to damages to the catalyst layer entailed by carbon corrosion (i.e., to the increase of the cathode electronic resistance). This is confirmed by the simultaneous decrease of the double layer capacity (Fig. 15b) near the hydrogen outlet, which is interpreted as a loss of electrochemically active area. Note that the impedance of the segments located in the centre of the cell or close to the opposite end shows no significant variation.

4. Conclusion

A method based on the analysis of local current densities measured in a segmented cell is developed and used to estimate carbon oxidation during fuel cell start-up. The results show clearly that the rate at which hydrogen is introduced into the anode compartment has a significant impact on fuel cell durability: it must be as high as possible in the presence of air or oxygen. Similarly, if air has to be introduced into the anode compartment at shut-down, its flow rate must be as high as possible.

Introducing hydrogen in an anode compartment initially occupied by air causes profound damage to the cathode, and this can entail a steep decrease of the fuel cell performance. Local electrochemical impedance spectroscopy measurements carried out on damaged MEA show that the segments that remain for the longest time in the presence of air (while the others are fed by hydrogen) are the most affected by carbon oxidation. Carbon oxidation occurs at the cathode, in the presence of negative currents. However, these negative currents have also a capacitive origin, which explains the fuel cell voltage overshoot observed during start-up. It is possible to evaluate the faradic and the capacitive contributions to the negative currents by comparing the value measured during start-up, in the presence of air in the anode compartment, and in the presence of nitrogen. In this last case, one can reasonably assume that the faradic contribution is negligible since no significant degradation occurs after a succession of start/stop sequences.

The results of this work should help optimising start-up and shut-down protocols in order to improve fuel cells durability. They can also be used to improve carbon oxidation models during start-up [26].

References

[1] C.A. Reiser, L. Bregoli, T.W. Patterson, J.S. Yi, Electrochemical and Solid-State Letters 8 (6) (2005) A273–A276.
[2] H. Tang, Z. Qi, M. Ramani, J.F. Elter, Journal of Power Sources 158 (2006) 1306–1312.
[3] N. Takeuchi, T.F. Fuller, Journal of the Electrochemical Society 155 (7) (2008) B770–B775.
[4] Z. Siroma, N. Fujiwara, T. Ioroi, S. Yamazaki, Journal of Power Sources 172 (2007) 155–162.
[5] J.P. Meyers, R.M. Darling, Journal of the Electrochemical Society 153 (8) (2006) A1432–A1442.
[6] J. Kim, J. Lee, Y. Tak, Journal of Power Sources 192 (2009) 674–678.
[7] W. Gu, R.N. Carter, P.T. Yu, H.U. Gasteiger, ECS Transactions 11 (1) (2007) 963–973.
[8] H. Chizawa, Y. Ogami, H. Naka, A. Matsunaga, N. Aoki, T. Aoki, ECS Transactions 3 (1) (2006) 645–655.
[9] A.B. Ofstad, J.R. Davey, S. Sunde, R.L. Borup, ECS Transactions 16 (2) (2008) 1301–1311.
[10] L.C. Pérez, L. Brandão, J.M. Sousa, A. Mendes, Renewable and Sustainable Energy Reviews 15 (2011) 169–185.
[11] S.A. Freunberger, M. Reum, J. Evertz, A. Wokaun, F.N. Büchi, Journal of the Electrochemical Society 153 (11) (2006) A2158–A2165.
[12] M. Reum, A. Wokaun, F.N. Büchi, Journal of the Electrochemical Society 156 (10) (2009) B1225–B1231.
[13] M. Reum, S.A. Freunberger, A. Wokaun, F.N. Büchi, Journal of the Electrochemical Society 156 (3) (2009) B301–B310.
[14] F.-B. Weng, C.-Y. Hsu, C.-W. Li, International Journal of Hydrogen Energy 35 (2010) 3664–3675.
[15] Z. Siroma, J. Takahashi, K. Yasuda, K. Tanimoto, M. Inaba, A. Tasaka, ECS Transactions 3 (1) (2006) 1041–1047.
[16] D.J.L. Brett, S. Atkins, N.P. Brandon, V. Vesovic, N. Vasileiadis, A.R. Kucernak, Electrochemistry Communication 3 (2001) 628–632.
[17] G. Maranzana, C. Moyne, J. Dillet, S. Didierjean, O. Lottin, Journal of Power sources 195 (2010) 5990–5995.
[18] Q. Shen, M. Hou, D. Liang, Z. Zhou, X. Li, Z. Shao, B. Yi, Journal of Power Sources 189 (2009) 1114–1119.
[19] S. Gottesfeld, J. Pafford, Journal of the Electrochemical Society 135 (1988) 2651.
[20] T.E. Springer, T. Rockward, T.A. Zawodzinski, S. Gottesfeld, Journal of the Electrochemical Society 148 (1) (2001) A11–A23.
[21] K.K. Bhatia, C.-Y. Wang, Electrochimica Acta 49 (2004) 2333–2341.
[22] S. Jiménez, J. Soler, R.X. Valenzuela, L. Daza, Journal of Power Sources 151 (2005) 69–73.
[23] P.J. Ferreira, G.J. la O', Y. Shao-Horn, D. Morgan, R. Makharia, S. Kocha, H.A. Gasteiger c, Journal of the Electrochemical Society 152 (11) (2005) A2256–A2271.
[24] F.H. Garzon, J.R. Davey, R.L. Borup, ECS Transactions 1 (8) (2006) 153–166.
[25] J. Mainka, G. Maranzana, J. Dillet, S. Didierjean, O. Lottin, Proceedings WHEC 18, Energie Agentur, NRW, Germany, 2010.
[26] J. Hu, P.C. Sui, S. Kumar, N. Djilali, Electrochimica Acta 54 (2009) 5583–5592.